Stochastic transport of high-energy particles through a turbulent plasma

L. Chen, A. Bott, P. Tzeferacos, A. Rigby, A. Bell, R. Bingham, C. Graziani, J. Katz, C. Li, M. Koenig, et al.

Stochastic transport of high-energy particles through a turbulent plasma

L. E. Chen[1], A. F. A. Bott[1], P. Tzeferacos[1,2], A. Rigby[1], A. Bell[1], R. Bingham[3,4], C. Graziani[5], J. Katz[6], M. Koenig[7], C. K. Li[8], R. Petrasso[8], H.-S. Park[9], J. S. Ross[9], D. Ryu[10], D. Ryutov[9], T. G. White[1,11], B. Reville[12], J. Matthews[1], J. Meinecke[1], F. Miniati[1], E. G. Zweibel[13], S. Sarkar[1,14], A. A. Schekochihin[1], D. Q. Lamb[2], D. H. Froula[5], G. Gregori[1,2]

[1]*Department of Physics, University of Oxford, Oxford, UK*

[2]*Department of Astronomy and Astrophysics, University of Chicago, Chicago, IL, USA*

[3]*Rutherford Appleton Laboratory, Didcot, UK*

[4]*Department of Physics, University of Strathclyde, Glasgow, UK*

[5]*Argonne National Laboratory, Mathematics and Computer Science Division, Argonne, IL, USA*

[6]*Laboratory for Laser Energetics, University of Rochester, Rochester, NY, USA*

[7]*Laboratoire pour l'Utilisation de Lasers Intenses, CNRS CEA, France*

[8]*Massachusetts Institute of Technology, Cambridge, MA, USA*

[9]*Lawrence Livermore National Laboratory, Livermore, CA, USA*

[10]*Department of Physics, School of Natural Sciences, UNIST, Ulsan, Korea*

[11]*Department of Physics, University of Nevada, Reno, NV, USA*

[12]*School of Mathematics and Physics, Queens University Belfast, UK*

[13]*Departments of Astronomy and Physics, University of Wisconsin, Madison, WI, USA*

[14]*Niels Bohr Institute, Copenhagen, Denmark*

The interplay between charged particles and turbulent magnetic fields is crucial to understanding how cosmic rays propagate through space[1]. A key parameter which controls this interplay is the ratio of the particle gyroradius to the correlation length of the magnetic turbulence. For the vast majority of cosmic rays detected at the Earth, this parameter is small, and the particles are well confined by the Galactic magnetic field. But for cosmic rays more energetic than about 30 EeV, this parameter is large. These highest energy particles are not confined to the Milky Way and are presumed to be extragalactic in origin. Identifying their sources requires understanding how they are deflected by the intergalactic magnetic field[2], which appears to be weak, turbulent with an unknown correlation length, and possibly spatially intermittent. This is particularly relevant given the recent detection by the Pierre Auger Observatory of a significant dipole anisotropy in the arrival directions of cosmic rays of energy above 8 EeV[3]. Here we report measurements of energetic-particle propagation through a random magnetic field in a laser-produced plasma. We characterize the diffusive transport of these particles and recover experimentally pitch-angle scattering measurements and extrapolate to find their mean free path and the associated diffusion coefficient, which show scaling-relations consistent with theoretical studies[4,5]. This experiment validates these theoretical tools for analyzing the propagation of ultra-high energy cosmic rays through the intergalactic medium[6].

Faithfully representing the propagation of energetic charged particles in structured electromagnetic fields is a key challenge in plasma physics. The interaction of cosmic rays with magnetic turbulence controls their confinement time, their energy and momentum exchange with the thermal

gas, and their radiative emission[7,8].

A theoretical framework has been developed for studying energetic-particle propagation, based on direct numerical simulations of particle orbits and complemented by statistical techniques (see Reference[1] for a review). In particular, it was shown by Jokipii[9] that random, small-amplitude fluctuations of the magnetic field superimposed on a mean background field lead to diffusive particle propagation. This is a cornerstone of cosmic-ray transport theory, but is by no means to be taken for granted: certain forms of magnetic-field structure lead to anomalous diffusion[10–12].

Particle diffusion is a fundamental effect associated with turbulence, and therefore laboratory experiments can provide a wealth of data to expand our present understanding of the process[13–15]. Past experiments on particle transport in diffuse laboratory plasmas with strong mean magnetic fields have provided some insights[16–19], but the important case of particle propagation in a fully stochastic magnetic field, i.e., with a zero mean background magnetic field, $\langle \boldsymbol{B} \rangle = 0$, and under conditions of weak magnetization, i.e., with Larmor radii much larger than the system size, has remained unstudied. This regime is of particular interest because, in perturbation theory, particles in a uniform background magnetic field follow zeroth order helical trajectories; however, in the formal limit $\langle \boldsymbol{B} \rangle \to 0$ the solutions become non-trivial[20].

To fill this gap and generate a high-velocity, weakly-magnetized, turbulent plasma, we employ the colliding-plasma platform, developed previously by Tzeferacos et al.[21,22] to study fluctuation dynamo (see Fig. 1 for details). Three-dimensional simulations with the radiation-magnetohydrodynamics code FLASH[23] guided and informed this experimental design, including details of the targets and

the grids, and the timing of the diagnostics[21].

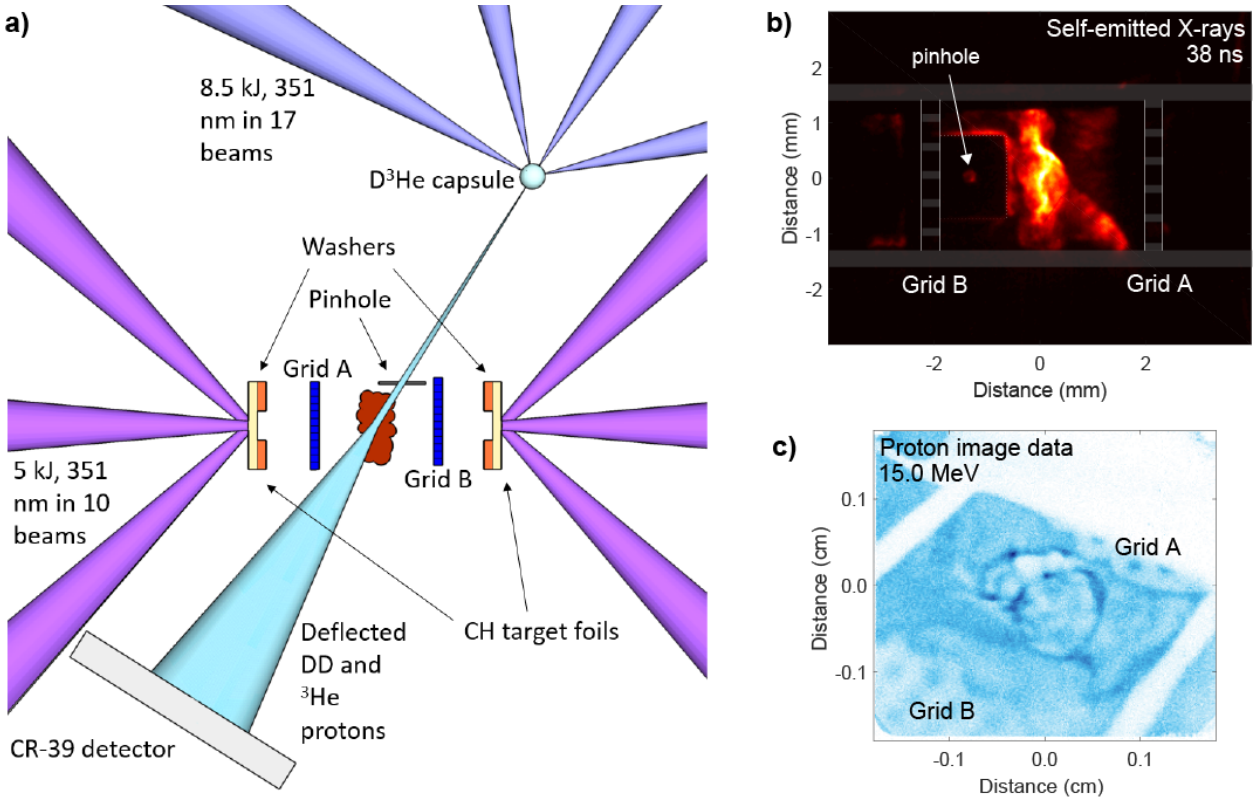

Figure 1: **Experimental setup**. **a)** Two 50 μm thick CH foils attached to a pair of 230 μm thick CH washers (with 400 μm diameter wells to act as collimators) and two grids (comprised of periodic 300 μm holes and 100 μm wires) are placed 8 and 4 mm apart, respectively. Each foil is irradiated with 5 kJ of energy during a 10 ns pulse (10 frequency-tripled laser beams on each foil). This produces two counter-propagating plasma flows which subsequently pass through a pair of grids. The two flows then meet, shear each other, and become turbulent in the central region between the two grids (the interaction region). A 420 μm diameter, 2 μm SiO_2 thick shell capsule, filled with 18 atm D^3He gas (6 atm ^2D and 12 atm ^3He), is placed 10 mm away from the interaction region. The capsule is imploded using 17 additional beams (frequency-tripled to 351 nm, providing 270 J/beam for a 1 ns pulse) to produce 3.3 and 15 MeV fusion protons [24,25]. A 300 μm diameter pinhole is placed between the capsule and the interaction region in selected shots. The protons are detected on the opposite side of the capsule with a nuclear track detector (CR-39) film pack 27 cm from the plasma interaction region, achieving a magnification of $\times$28. **b)** X-ray self-emission from the interaction region at t = 38 ns after the start of the laser drive from a shot without the pinhole. **c)** 15 MeV proton image of entire interaction region at 38 ns, without pinhole shield present in the path. For clarity, the image scale is shown with the magnification removed.

The electron density and temperature are measured using collective Thomson scattering (see Katz et al.[26] and Supplementary Information) and found to be $n_e \simeq 9 \times 10^{19}$ cm^{-3} and $T_e \simeq 400$ eV immediately after the flow collision (at about 27 ns after the start of the drive). The mean flow velocity (u_{flow}) and the turbulent velocity (u_{turb}) of the flow are also obtained by this diagnostic. Prior to collision, the counter-propagating flows reach velocities of $u_{flow} \simeq 200\,\mathrm{km\,s^{-1}}$, whereas

in the turbulent region at late times we measure $u_{flow} \simeq 50\,\mathrm{km\,s^{-1}}$ and $u_{turb} \simeq 100\,\mathrm{km\,s^{-1}}$ at the driving-scale ($L \simeq 400$ μm, set by the grid spacing and confirmed by X-ray images of the turbulence).

Fig. 1b shows the plasma emission in the soft X-ray region at 38 ns after the start of the laser drive. As discussed in Tzeferacos et al.[22], fluctuations in the emissivity of such a plasma can be related to fluctuations of density[27]. They exhibit a characteristic Kolmogorov power-law spectrum (Fig. 4d). The presence of a stochastic magnetic field generated by turbulence[21,22] is inferred using proton radiography. Fig. 1c shows a proton radiograph of the plasma corresponding to the same time as the X-ray image in Fig. 1b. The presence of strong inhomogeneities in the proton flux and the stochastic, non-regular morphology of the structures is due to protons being deflected by strong, tangled magnetic fields.

To probe the diffusive transport of particles through the turbulent plasma we modified our experimental platform to introduce a collimated proton beam. The collimation was achieved by placing a 200 μm thick aluminum shield between the D^{3}He capsule and the interaction region, with a 300 μm diameter pinhole (shown in Fig. 1a). The pinhole imprint is recorded on the detector plane, as shown in Fig. 2. The proton-beam imprints appear deformed and broadened due to diffusion of the protons through the turbulent magnetized plasma. The proton-beam imprint contours are shown in Figs. 3a and 3b. The corresponding diffusive deflection velocities, $\Delta v_\perp$, as interpreted from the scattering angle $|\Delta v_\perp|/V$, where V is the proton-beam speed, are shown in Fig. 3c (see also Supplementary Information). We have performed radiation magneto-

hydrodynamic simulations of the full experiment using the FLASH code[21]. From the simulation results, proton trajectories and resultant transverse deflection as they cross the interaction region have also been calculated and are in good agreement with the experimental measurements (Fig. 3c and additional details in the Supplementary Information).

The velocity deflections due to magnetic fields scale independently of velocity, whereas those due to electric fields scale as $\sim 1/V$ (shown in the Supplementary Information). The near-equality of the deflection velocities of the two proton species, evident in Fig. 3c, suggests that scattering is predominantly due to magnetic fields. While there are many possible processes that could lead to the scattering of a charged-particle beam passing through the turbulent plasma, for our experiment we argue that most are negligible (see Supplementary Information), on account of the low density of the plasma and the large speed of the protons compared to driving-scale plasma motions. Detailed calculations and descriptions of possible electric field effects are given in the Supplementary Information.

From our experimental measurement of $\Delta v_\perp$, we can calculate the associated angular scattering coefficient in velocity-space, $\nu \sim (\Delta v_\perp/V)^2/\tau$, where $\tau = \ell_i/V$ is the transit time of the particles through the plasma. For a plasma on the scale of $L \gg V/\nu$, our results imply an isotropic spatial diffusion coefficient $\kappa \sim V^2/\nu = \ell_i V^3/(\Delta v_\perp)^2$. Since κ/V^3 is constant in our experiment (Fig. 3d), it means $(\Delta v_\perp)^2 \propto \ell_i \propto \tau$. This is indeed consistent with a normal (Markovian) spatial diffusion[1,5,20].

From the flux inhomogeneities observed in the proton image (see e.g., Fig. 1c), an exper-

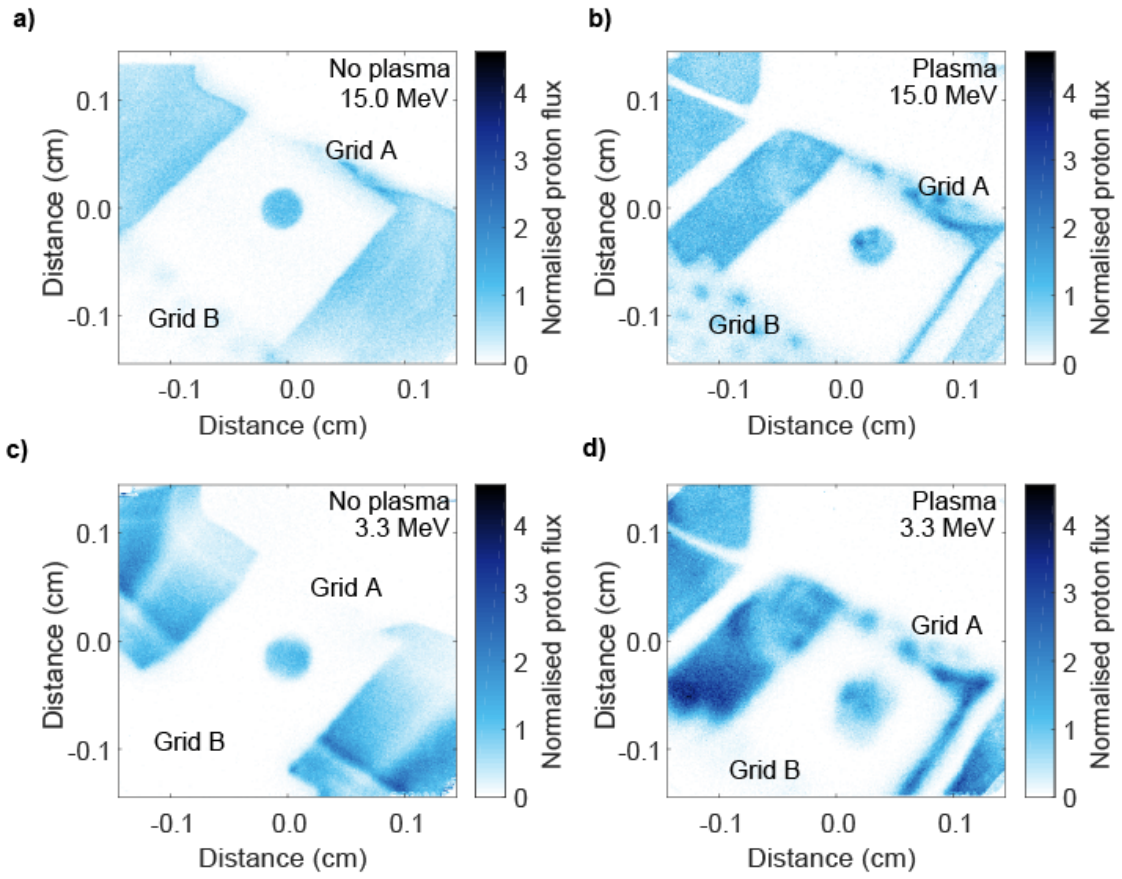

Figure 2: **Proton pinhole images.** Radiographs obtained on the CR-39 film pack with proton energies of **a)** 15 MeV, with no plasma in the interaction region, and **b)** 15 MeV, with a turbulent plasma in the interaction region. **c)** Same as **a)** but for the 3.3 MeV protons. **d)** Same as **b)** but for the 3.3 MeV protons. The pinhole shield is clearly seen to block most of the incoming proton flux from the capsule and, in the case where no plasma was present (**a)** and **c)**), it produces a fixed 300 μm diameter beam of 3.3 and 15 MeV protons that passes through to the detector. For the case when a plasma is present in the interaction region (**b)** and **d)**), the beam is deformed and broadened before reaching the detector.

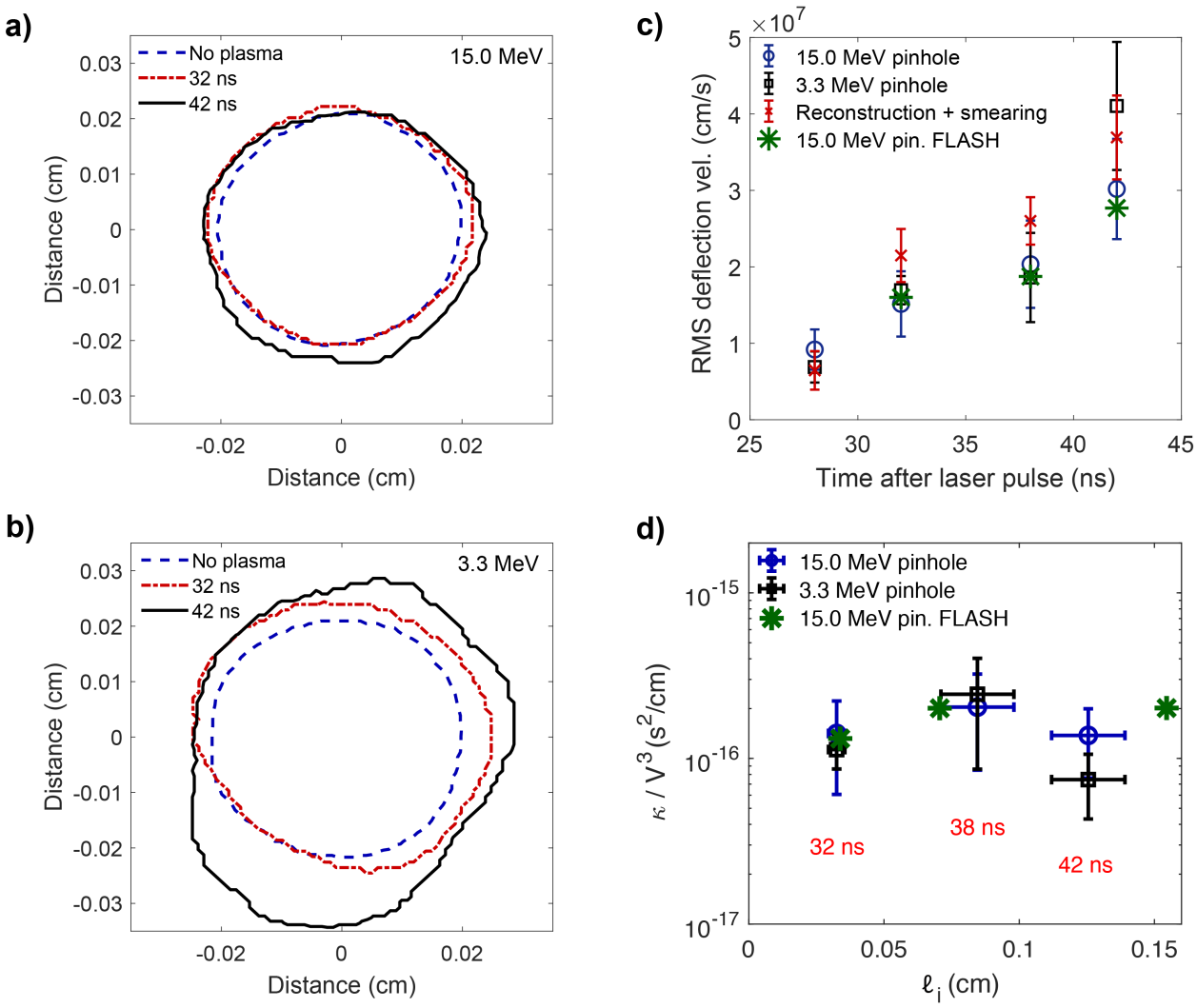

Figure 3: **Diffusive scattering of the proton beam.** Contours of the beam imprint on the CR-39 plate for **a)** 15 MeV protons and **b)** 3.3 MeV protons, taken with different delay times after the start of the drive beams. **c)** The RMS transverse deflection velocity acquired by the proton beam, calculated using the inferred reconstruction and smearing algorithm, the contour analysis of the pinhole image (for both proton species), and evaluated using FLASH simulations. **d)** Measured spatial diffusion coefficient as a function of the plasma interaction length, as determined from the X-ray self-emission images and the 15 MeV pinhole synthetic radiographs from the FLASH simulations.

imental radiograph can be inverted[28,29] to give the path-integrated magnetic field. By using this inversion technique to compare the 3.3 MeV and 15 MeV proton images, we also find evidence that smaller-scale fluctuations diffusively scatter the proton beam. We show in the Supplementary Information that the path-integrated magnetic fields experienced by each of these beams are essentially the same. As a result, the 15 MeV proton radiograph in Fig. 1c can be processed to find the path-integrated magnetic field (Fig. 4a), which is then used to generate a synthetic 3.3 MeV proton image (Fig. 4b). Comparing this image with the true experimental 3.3 MeV proton radiograph (shown in Fig. 4c), we observe that the flux inhomogeneities associated with the driving-scale magnetic structures are more smeared in the experimental data. This is consistent with the presence of small-scale fields causing diffusive scattering of the proton beam, which smooths and obscures the detection of small-scale structures (for more details, see the Supplementary Information). The corresponding deflection angles, $\Delta v_\perp/V$, associated to this image-smearing effect (combined with the deflections by large-scale fields) are shown in Fig. 3c, which, in fact, agree closely with the deflection angles obtained from the pinhole method described above.

A possible explanation of the observed smearing is that it arises due to stochastic magnetic fields. Using characteristic values for the plasma properties corresponding to 38 ns delay (see Supplementary Information for calculations of these values), we take the size of the interaction region to be $\ell_i \sim 1\,\mathrm{mm}$, as inferred from the X-ray images. The root-mean-square (RMS) of the magnetic field is determined from the reconstructed path-integrated magnetic field[22] giving $B_{rms} \sim 80\,\mathrm{kG}$. While this value of B_{rms} is dependent on the magnetic energy power-law spectrum shown in Fig. 4d, and thus on the resolution of the proton images, for a dynamo-driven

magnetic field, such dependence is rather weak. This is because most of the magnetic energy is contained within the largest filaments[22]. The value of the correlation length, instead, is more difficult to evaluate from the experimental images, since small-scale structures are unresolved. From the FLASH simulations we find that the characteristic size is $\ell_B \sim 50\,\mu\mathrm{m}$, corresponding to the largest unresolved magnetic field structures. For the case of normal diffusion, a random-walk argument gives $\Delta v_\perp \approx q_e B_{rms}\sqrt{\ell_i \ell_B}/m_p \sim 1.7 \times 10^7\,\mathrm{cm\,s^{-1}}$ (see Supplementary Information for full derivation) where m_p is the mass of a proton. This is consistent with the measured RMS deflection velocity (Fig. 3c). Further, since the values of V, B_{rms}, and the power spectrum of the magnetic energy (and therefore the value of ℓ_B) do not change in the experiment after the magnetic-field amplification saturates[21,22], the random walk model also predicts a constant $\kappa/V^3 \sim m_p^2/(q_e B_{rms})^2 \ell_B \simeq 3 \times 10^{-16}\,\mathrm{s^2\,cm^{-1}}$, in agreement with the values shown in Fig. 3d.

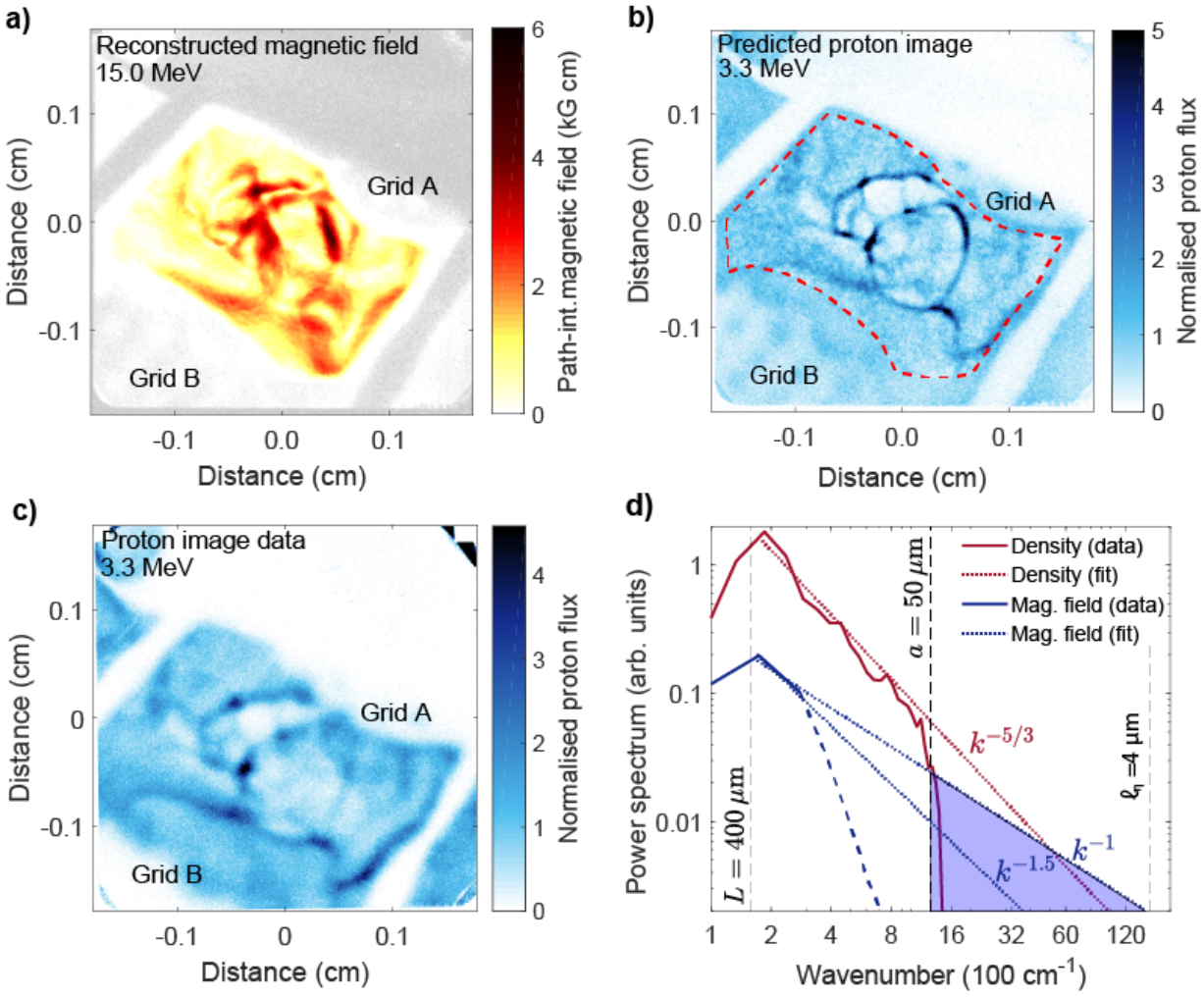
a)
Reconstructed magnetic field
15.0 MeV
Grid A
Grid B
Distance (cm)
Path-int.magnetic field (kG cm)
b)
Predicted proton image
3.3 MeV
Grid A
Grid B
Distance (cm)
Normalised proton flux
c)
Proton image data
3.3 MeV
Grid A
Grid B
Distance (cm)
Normalised proton flux
d)
Density (data)
Density (fit)
Mag. field (data)
Mag. field (fit)
$a = 50\,\mu$m
$L = 400\,\mu$m
$\ell_\eta = 4\,\mu$m
$k^{-5/3}$
k^{-1}
$k^{-1.5}$
Power spectrum (arb. units)
Wavenumber (100 cm^{-1})

142

Figure 4: **Magnetic field reconstruction. a)** Large-scale path-integrated magnetic field reconstructed from the 15 MeV proton image in Fig. 1c. **b)** 3.3 MeV proton image predicted by assuming 3.3 MeV protons experience the same path-integrated field as the 15 MeV protons, with additional blurring to account for the finite source size. **c)** Experimental 3.3 MeV proton image taken at $t = 38$ ns. **d)** Density (red, solid) and magnetic-energy (blue, solid and long-dashed) spectra in the turbulent plasma at $t = 38$ ns as measured from self-emitted X-rays and proton imaging, respectively. The experimental spectra are plotted alongside power-law fits (red, dashed for density; blue, dashed for magnetic energy) extended down to the viscous ($\ell_{\nu_c} \simeq 5$ μm) and resistive ($\ell_\eta \simeq 4$ μm) dissipation scales. Turbulent dynamo is expected to generate magnetic fields over a range of scales (the relevant physical scales are summarized in the Supplementary Information), from driving scales down to the resistive scale, $\ell_\eta \simeq 4$ μm. However, due to the finite size of the proton source, the spatial resolution of the proton radiograph is 45 μm; similarly, the resolution of the X-ray framing camera is 50 μm. Magnetic-field structures with sufficiently small wavelengths (blue shaded region) affect the dynamics of the proton beam diffusively. This accounts for why we do not see the expected magnetic-energy spectrum for a dynamo-driven magnetic field, which is believed to have a dependence on wavenumber within the range $\sim k^{-1} - k^{-3/2}$ (where k is the spatial wavenumber) [22,30].

For isotropic statistics and $r_g \gg \ell_B$ (r_g is the gyroradius of the protons), the proton mean free path is given by $\lambda \simeq V/\nu \simeq 10^4\,\mathrm{cm}$. In this regime, both a simple random walk argument and the theory and simulations of Subedi et al.[5] predict a scaling $\lambda \propto r_g^2/\ell_B$. Since $r_g/\ell_B \simeq 1,380$ for the 15 MeV and $\simeq 650$ for the 3.3 MeV protons, we can use this scaling to extrapolate from

Subedi et al. a ratio $\lambda/\ell_B \simeq 1 - 3 \times 10^6$, which is consistent with the experimental values that we obtain within a factor of unity ($\lambda/\ell_B \simeq 2 \times 10^6$ in the experiment). This agreement provides experimental evidence of the $\lambda \propto r_g^2/\ell_B$ scaling in the large r_g/ℓ_B regime.

These results are relevant to our current understanding of cosmic ray propagation for energies beyond $\sim$ 30 EeV in the intergalactic medium [6]. This validates a critical tool for interpreting anisotropies and constraining the directions and distances to sources in the framework of the turbulent intergalactic magnetic field model. This is especially timely given the recent detection by the Pierre Auger Observatory of a significant dipole anisotropy in the arrival directions of cosmic rays of energy above 8 EeV [3].

Supplementary Information is available in the online version of the paper.

Acknowledgements The research leading to these results has received funding from the European Research Council under the European Community's Seventh Framework Programme (FP7/2007-2013) / ERC grant agreements no. 256973 and 247039, the U.S. Department of Energy under Contract No. B591485 to Lawrence Livermore National Laboratory, Field Work Proposal No. 57789 to Argonne National Laboratory, and grants no. DE-NA0002724, DE-NA0003605, and DE-SC0016566 to the University of Chicago. We acknowledge support from the National Science Foundation under grants PHY-1619573 and AST-1616037 and from Department of Energy Cooperative Agreement No. DE-NA0001944 to the University of Rochester. Awards of computer time were provided by the U.S. Department of Energy ASCR Leadership Computing Challenge (ALCC) program. This research used resources of the Argonne Leadership Computing Facility

168 at Argonne National Laboratory, which is supported by the Office of Science of the U.S. Depart-
169 ment of Energy under contract DE-AC02-06CH11357. Support from AWE plc., the Engineer-
170 ing and Physical Sciences Research Council (grant numbers EP/M022331/1, EP/N014472/1 and
171 EP/P010059/1) and the Science and Technology Facilities Council of the United Kingdom is also
172 acknowledged, as well as funding from grants 2016R1A5A1013277 and 2017R1A2A1A05071429
173 of the National Research Foundation of Korea. J. Matthews, A. Bell and G. Gregori would like
174 to thank Prof Katherine Blundell (University of Oxford) for stimulating discussions on cosmic ray
175 measurements.

176 **Author Contributions** L.E.C., A.F.A.B., J.K., P.T., A.R., D.Q.L., H.-S.P., J.S.R., C.K.L. and G.G.
177 attended the experimental campaigns, which were supported by A.B., R.B., M.K., R.P., D.Ryu,
178 D.Ryutov., T.G.W., B.R., J.Matthews, J.Meinecke, F.M., S.S., A.A.S, and D.H.F.; P.T. performed
179 the simulations; A.F.A.B., A.B., R.B., C.G., D.R., D.R., B.R., J.Matthews, E.G.Z., S.S., and A.A.S.
180 supervised the development of theory. This project was conceived by G.G., P.T. and D.Q.L. All
181 authors wrote the manuscript.

182 **Author Information** Reprints and permssions information is available at www.nature.com/reprints.
183 The authors declare competing financial interests: details are available in the online version of the
184 paper. Readers are welcome to comment on the online version of the paper. Correspondence
185 and requests for materials should be addressed to L.E.C. (laura.chen@physics.ox.ac.uk) or G.G.
186 (gianluca.gregori@physics.ox.ac.uk).

187 **Reviewer Information** *Nature* thanks the anonymous reviewer(s) for their contribution to the peer

review of this work.

1. Shalchi, A. *Nonlinear Cosmic Ray Diffusion Theories* (Springer, 2009).

2. Kotera, K. & Olinto, A. V. The Astrophysics of Ultrahigh Energy Cosmic Rays. *Annual Review of Astronomy and Astrophysics* **49**, 119–153 (2010).

3. The Pierre Auger Collaboration. Observation of a large-scale anisotropy in the arrival directions of cosmic rays above 8×10^{18}eV. *Science* **357**, 1266–1270 (2017).

4. Dolginov, A. & Toptygin, I. Multiple Scattering of Particles in a Magnetic Field with Random Inhomogeneities. *Journal of Experimental and Theoretical Physics* **24**, 1195 (1967).

5. Subedi, P. *et al.* Charged Particle Diffusion in Isotropic Random Magnetic Fields. *The Astrophysical Journal* **837**, 140 (2017).

6. Kotera, K. & Lemoine, M. Optical depth of the Universe to ultrahigh energy cosmic ray scattering in the magnetized large scale structure. *Physical Review D* **77**, 123003 (2008).

7. Grenier, I. A., Black, J. H. & Strong, A. W. The Nine Lives of Cosmic Rays in Galaxies. *Annual Review of Astronomy and Astrophysics* **53**, 199–246 (2015).

8. Zweibel, E. G. The basis for cosmic ray feedback: Written on the wind. *Physics of Plasmas* **24**, 055402 (2017).

9. Jokipii, J. R. Cosmic-ray propagation. I. Charged particles in a random magnetic field. *The Astrophysical Journal* **146**, 480–487 (1966).

10. Jokipii, J. R. & Parker, E. N. Cosmic-ray life and the stochastic nature of the galactic magnetic field. *The Astrophysical Journal* **155**, 799–806 (1969).

11. Reville, B., O'Sullivan, S., Duffy, P. & Kirk, J. G. The transport of cosmic rays in self-excited magnetic turbulence. *Monthly Notices of the Royal Astronomical Society* **386**, 509–515 (2008).

12. Lazarian, A. & Yan, H. Superdiffusion of cosmic rays: Implications for cosmic ray acceleration. *The Astrophysical Journal* **784** (2014).

13. Remington, B. A., Arnett, D., Drake, R. P. & Takabe, H. Modeling Astrophysical Phenomena in the Laboratory with Intense Lasers. *Science* **284**, 1488–1493 (1999).

14. Ryutov, D. D., Remington, B. A., Robey, H. F. & Drake, R. P. Magnetohydrodynamic scaling: From astrophysics to the laboratory. *Physics of Plasmas* **8**, 1804–1816 (2001).

15. Kuramitsu, Y. *et al.* Laboratory investigations on the origins of cosmic rays. *Plasma Physics and Controlled Fusion* **54**, 124049 (2012).

16. Gustafson, K., Ricci, P., Furno, I. & Fasoli, A. Nondiffusive suprathermal ion transport in simple magnetized toroidal plasmas. *Physical Review Letters* **108**, 035006 (2012).

17. Anderson, J. K. *et al.* Fast ion confinement and stability in a neutral beam injected reversed field pinch. *Physics of Plasmas* **20**, 056102 (2013).

18. Furno, I. *et al.* Plasma turbulence, suprathermal ion dynamics and code validation on the basic plasma physics device TORPEX. *Journal of Plasma Physics* **81**, 345810301 (2015).

19. Bovet, A., Fasoli, A., Ricci, P., Furno, I. & Gustafson, K. Nondiffusive transport regimes for suprathermal ions in turbulent plasmas. *Physical Review E* **91**, 041101 (2015).

20. Tsytovich, V. N. *Theory of Turbulent Plasma* (Consultants Bureau, 1977).

21. Tzeferacos, P. *et al.* Numerical modeling of laser-driven experiments aiming to demonstrate magnetic field amplification via turbulent dynamo. *Physics of Plasmas* **24**, 041404 (2017).

22. Tzeferacos, P. *et al.* Laboratory evidence of dynamo amplification of magnetic fields in a turbulent plasma. *Nature Communications* **9**, 591 (2018).

23. Tzeferacos, P. *et al.* FLASH MHD simulations of experiments that study shock-generated magnetic fields. *High Energy Density Physics* **17**, 24–31 (2015).

24. Li, C. K. *et al.* Measuring E and B fields in laser-produced plasmas with monoenergetic proton radiography. *Physical Review Letters* **97**, 135003 (2006).

25. Kugland, N. L., Ryutov, D. D., Plechaty, C., Ross, J. S. & Park, H. S. Invited Article: Relation between electric and magnetic field structures and their proton-beam images. *Review of Scientific Instruments* **83**, 101301 (2012).

26. Katz, J. *et al.* A reflective optical transport system for ultraviolet Thomson scattering from electron plasma waves on OMEGA. *Review of Scientific Instruments* **83**, 10349 (2012).

27. Churazov, E. *et al.* X-ray surface brightness and gas density fluctuations in the Coma cluster. *Monthly Notices of the Royal Astronomical Society* **421**, 1123–1135 (2012).

28. Graziani, C., Tzeferacos, P., Lamb, D. Q. & Li, C. Inferring morphology and strength of magnetic fields from proton radiographs. *Review of Scientific Instruments* **88**, 123507 (2017).

29. Bott, A. F. A. *et al.* Proton imaging of stochastic magnetic fields. *Journal of Plasma Physics* **83**, 905830614 (2017).

30. Schekochihin, A. A. *et al.* Fluctuation dynamo and turbulent induction at low magnetic Prandtl numbers. *New Journal of Physics* **9** (2007).